Published in final edited form as:
Lab Chip. 2012 December 7; 12(23): 4976–4985. doi:10.1039/c2lc40338b.

Formation and Optogenetic Control of Engineered 3D Skeletal Muscle Bioactuators†

Mahmut Selman Sakar[a], **Devin Neal**[a], **Thomas Boudou**[b], **Michael A. Borochin**[b], **Yinqing Li**[c], **Ron Weiss**[c,d], **Roger D. Kamm**[a,d], **Christopher S. Chen**[b], and **H. Harry Asada**[a]

[a]Department of Mechanical Engineering, Massachusetts Institute of Technology, Cambridge, MA 02139

[b]Department of Bioengineering, University of Pennsylvania, Philadelphia, PA 19104

[c]Department of Electrical Engineering and Computer Science, Massachusetts Institute of Technology, Cambridge, MA 02139

[d]Department of Biological Engineering, Massachusetts Institute of Technology, Cambridge, MA 02139

Abstract

Densely arrayed skeletal myotubes are activated individually and as a group using precise optical stimulation with high spatiotemporal resolution. Skeletal muscle myoblasts are genetically encoded to express light-activated cation channel, Channelrhodopsin-2, which allows for spatiotemporal coordination of the multitude of skeletal myotubes that contract in response to pulsed blue light. Furthermore, ensembles of mature functional 3D muscle microtissues have been formed from the optogenetically encoded myoblasts using a high-throughput device. The device, called “skeletal muscle on a chip”, not only provides the myoblasts with controlled stress and constraints necessary for muscle alignment, fusion and maturation, but also facilitates to measure forces and characterize the muscle tissue. We measured the specific static and dynamic stresses generated by the microtissues, and characterized the morphology and alignment of the myotubes within the constructs. The device allows for testing the effect of a wide range of parameters (cell source, matrix composition, microtissue geometry, auxotonic load, growth factors, and exercise) on the maturation, structure, and function of the engineered muscle tissues in a combinatorial manner. Our studies integrate tools from optogenetics and microelectromechanical systems (MEMS) technology with skeletal muscle tissue engineering to open up opportunities to generate soft robots actuated by multitude of spatiotemporally coordinated 3D skeletal muscle microtissues.

Introduction

Locomotion is a key feature to animal survival and it involves the coordination of a large number of muscles in space and time. Animals perform a variety of complex movements such as flying and swimming by oscillating their wings or undulating their bodies with high spatiotemporal coordination. They adapt their locomotive gaits to their physical surroundings and navigate different environments by continuously changing the patterns of muscle activity (1). Muscle is an efficient actuator having superior power-to-weight ratio, force-to-weight ratio, compliance, plasticity, scalability and controllability when compared with traditional robotic actuators (2). Engineered muscle tissues *in vitro* have the potential to

†Electronic supplementary information (ESI) available.

Correspondence to: H. Harry Asada.

replicate some of these performance characteristics of their *in vivo* counterparts and serve as powering units for soft robotic devices demonstrating life-like mobility (3–5).

Previous work addressed the integration of engineered muscles with synthetic structures to develop functional biological machines (4–10). These biohybrid constructs display biomimetric functionality (5–7), and can even mimic the propulsion mechanism of jellyfish (4). The basic design principle of these devices is to form a self-assembled 2D cardiac muscle tissue on elastic surfaces. The synchronous contraction of muscle cells causes the substrate to bend and take 3D conformations. Skeletal muscle has several features making it more favorable than cardiac muscle for the production and regulation of force for locomotion (11). The organization of skeletal muscle is modular, having many longitudinally aligned, multinucleated muscle fibers assembled together by connective tissue to form a densely packed structure (12). By adjusting the number of muscle fibers contracting within a muscle and the tension developed by each contracting fiber, the nervous system effectively achieves controlled, graded tension. To achieve this selectivity, motoneurons innervate skeletal muscle cells at very localized regions called neuromuscular junctions (13). The variability in the arrangement of connections among multiple muscle units combined with precise spatiotemporal activation of individual units generates a wide range of motions (14).

The real potential of engineered skeletal muscle as a multi-degree of freedom, scalable, and robust actuator can be revealed with the formation of 3D anisotropic tissue-level organization and the application of neuron-like targeted stimulation protocols. Electrical stimulation techniques offer activation of excitable cells with precise timing but the spatial resolution of extracellular electrode arrays is limited. Intracellular electrodes can target specific muscle cells (15) but the electrodes should be either directly attached or placed in close proximity to the muscle fibers, which limits the type of activation patterns and the mechanical design of the mobile constructs. Optogenetics enable fast, precise, and localized stimulation of genetically engineered excitable cells in vitro and in vivo (16, 17). The minimally invasive and targeted nature of photostimulation makes it possible to control muscle activity in real-time even in freely behaving animals (17–22).

The current work aims to accomplish photostimulation of 3D skeletal muscle microtissues for spatiotemporally precise coordination of multiple muscle units. Functional hydrogel-based skeletal muscle tissues with dense, aligned and highly differentiated muscle fibers have been engineered in several different bioreactors for various different applications (23–33). Recent work addressed methods to control the final 3D tissue architecture using microfabrication technology (33–35), but still little quantitative data are available on the mechanical and chemical factors affecting the structure and function of individual cells inside the tissue. Understanding myogenesis, examining the mechanical interplay between muscle cells and the surrounding extracellular matrix during development, and performing combinatorial perturbation experiments (applying different mechanical and soluble stimuli and excitation protocols) are important requirements for optimizing the performance of engineered actuators especially for microscale applications. A high-throughput, miniaturized platform that allows monitoring of cell-matrix interactions as well as changes in myofiber morphology and rapid recording of microtissue force generation can characterize these properties. This platform can also serve as a skeletal muscle on a chip analogous to heart on a chip for tissue-level pharmacological studies (36, 37).

In our previous work, we introduced microfabricated tissue gauges (μTUGs), which simultaneously constrain and report forces generated by the microtissues in real-time (38, 39). Here, we integrate optical tools and transgenic expression of light-gated ion channels with this multi-purpose device to engineer light-activated, 3D skeletal muscle microtissues

and demonstrate multi-DOF motion. We first show that genetically engineered C2C12 murine muscle myoblasts expressing Channelrhodopsin-2 (ChR2) fuse to form functional myotubes on 2D surfaces and individual cells can be selectively activated with confined illumination. Once incorporated into our device, these myoblasts self-assemble and generate hundreds of 3D microtissues with longitudinally aligned and differentiated myofibers. The microtissues are activated upon exposure to brief light pulses, and we characterize the contractility of the tissue by monitoring the deformations of elastic microposts. With local stimulation, we demonstrate different modes of contraction patterns.

Results and Discussion

Development and optical stimulation of ChR2-expressing C2C12 myotubes

Skeletal muscle formation involves multiple distinct steps. Precursor cells called myoblasts proliferate, locally align and begin to fuse to form multinucleated myotubes. Myotubes grow in length and get thicker as more myoblasts merge with the developing fiber and the interior is filled with contractile proteins to form functional muscle fibers. Previous work showed that ChR2 enables temporally precise (tens of milliseconds) and spatially confined control of cardiac muscle contraction (17). A recent work reported the feasibility of optical control for skeletal muscle contractions (40). Here, we extend the results of this work by demonstrating selective activation of individual myotubes with confined illumination as well as formation, characterization and optical control of genetically engineered, 3D skeletal muscle microtissues. We generated a stable mouse skeletal muscle cell line (C2C12-ChR2) expressing ChR2-green fluorescent protein (GFP) fusion protein from the chicken β-actin promoter (CAG) using a non-viral strategy. Transfected myoblasts showed membrane-bound GFP signal (Fig. 1A), and they fused with each other to form ChR2-positive myotubes (Fig. 1B). Staining for muscle-specific protein α-actinin after 3 weeks in differentiation medium revealed striations indicative of sarcomeric structure and a sign of maturation (Fig. S2).

At day 10 of differentiation, application of pulsed blue light depolarized the cell membrane (Fig. S3) and induced cellular contractions in ChR2-positive myotubes, and did not induce contractions in non-transfected control myotubes. There is a non-linear, inverse relationship between the energy and the duration of light pulses required for the induction of muscle contractions (41). We observed repeatable and reliable myotube contractions with 20 ms pulses at 10 mW/mm^2 light intensity. Figure 1C shows a representative twitch profile induced by a single light pulse. The cells started to contract almost instantaneously, 17.3 ± 2.5 ms after light was turned on. Both ends of the myotubes were fixed onto the surface so we could not measure generated force. Instead, we tracked single points on the cell body to quantify the contractions, and normalized each point's displacement measurement with the maximum displacement of the point. The total duration of twitch (contraction and relaxation) showed great variability, ranging from 300 ms to more than a second as myotubes cultured on 2D surfaces have different levels of maturation.

Selective activation of C2C12-expressing myotubes using focused illumination

Next we investigated whether local stimulation induces contractions in functional myotubes. We generated light pulses with a diameter of 20 μm to selectively activate individual cells. For the tested fibers (n = 30 myotubes), pulsed illumination of one confined region (less than 10% of the total area of the cell) evoked contractile activity within the entire myotube body. The resulting twitch profile of local illumination closely resembles the profile generated by exposing the whole myotube with pulsed light at the same intensity (Fig. 1D). Based on this result, we generated a proof-of-concept experiment to demonstrate selective activation of myotubes using confined illumination (Fig. 1E and Movie S1). We selected 3

myotubes (M1, M2, and M3) located in close proximity. By changing the region of exposure (R1, R2, and R3), we activated single myotubes individually or multiple myotubes collectively (Fig. 1F). Thus, ChR2 can be used for precise local stimulation of myotubes *in vitro*.

Formation of 3D Muscle Tissues from ChR2-expressing myoblasts

Formation of functional skeletal muscle actuators requires structural organization at multiple length scales. The molecular level intracellular organization of myofibers is important for generating force effectively. The tissue level alignment of densely packed fibers inside the 3D muscle construct is critical for maximal transmission of the force throughout the muscle. To generate optically activated skeletal muscle microtissues demonstrating the basic contractile functionality, we fabricated T-shaped cantilevers incorporated inside arrays of micro-patterned wells within a PDMS mold (Fig. S4). The wells are filled with a suspension of genetically engineered myoblasts and liquid neutralized collagen I supplemented with Matrigel using a centrifugation-aspiration protocol (Fig. 2A). We chose collagen because it has been shown that naturally derived hydrogels undergo macroscale compaction when mixed with skeletal muscle myoblasts, which leads to high cell density and unidirectional cell alignment in the presence of engineered geometric constraints (32). The round myoblasts elongate, spread inside the polymerized gel and apply traction forces that spontaneously compact the matrix over time. Cells are distributed throughout the tissue, and the collective action of these local processes results in bulk contraction of the collagen gel. Elastic cantilevers restrict hydrogel compaction, and act as artificial tendons to anchor the skeletal muscle microtissues (SMTs) around the caps of the posts (Fig. 2B). Wide caps at the tips of the cantilevers ensure that microtissues do not slide off the top of the posts and remain anchored throughout the experiments. Using this reproducible fabrication technique, we generated a 10 × 13 array of 3D, free-standing constructs.

Remodeling and compaction of the matrix during the first 2 days of development in growth medium resulted in a marked reduction of construct size (final width 144.2 ± 6.4 μm at the thinnest portion of the construct) and a nearly 10-fold increase in the cell density. The densely packed cells were evenly distributed throughout the tissue and uniform GFP expression identified expression of ChR2 by almost all of the cells (Fig. 2C). The presence of cantilevers generates anisotropic boundary conditions inside the tissue, and the imposed stress on the matrix led to cell alignment (Fig. 2D). We previously showed that cytoskeletal tension corresponds to simulated stress gradients and actin filaments align in the direction of predicted principal stresses (38). Cells stretched out along stress gradients showed actin alignment and elongated nuclei morphology, which eventually led to patterned differentiation of myotubes during self-assembly by myoblasts. After switching to differentiation medium, aligned myoblasts start to fuse with each other, and extensive cytoskeletal reorganization occurs during this period. Visualization of F-actin protein inside the myotubes reveals the formation of arrays of parallel filaments along the cell body (Fig. 2E).

We fabricated cantilevers with different spring constants (k = 0.2–0.45 mN/mm) by varying the ratio between PDMS and curing agent (Fig 2F). Microtissues formed around relatively rigid posts exhibited significant thinning and high rates of rupture in the second week of culture. This is the time period when myotubes start to mature and contract spontaneously. As the stiffness of the cantilevers is decreased, the amount of deflection reaches a point where cantilevers start to show nonlinear responses, which causes a difficulty in force calibration. For this reason, we used cantilevers with an intermediate spring constant of 0.33 mN/mm for all the remaining experiments. By changing the dimensions of the cantilevers and the wells, we can control the final geometry of constructs. Wider posts result in thicker microtissues while increasing the interpost distance generates longer microtissues (Fig 2F).

Cell morphology, alignment and differentiation in SMTs

After 3 weeks in culture, staining for α-actinin showed multiple longitudinally aligned myotubes within each microtissue (Fig. 3). Even though microtissues had similar dimensions and number of myoblasts at the time of switching to differentiation medium, they ended up having different numbers of myotubes (Fig. 3A–C). The final size of the constructs allowed at most 3 myotubes to form on top of each other (Fig. 3B). They had 7 myotubes on average (data from 20 SMTs) and most of the myotubes had well-developed parallel cross-striations, consistent with sarcomeric structure (Fig. 3D). Average fiber diameter was 19.24 ± 2.62 μm (n = 140 myotubes from 20 SMTs), and they were as thick as 39 μm. The micrometer scale of the SMTs allows visualization of the fine-scale sarcomeric structure of the cells (Fig 3E) and reconstruction of the 3D muscle architecture of the whole microtissue (Fig. 3F) using confocal microscopy. Centimeter-scale constructs require histological sectioning to visualize the interior of the tissue, which is a significant obstacle for high-throughput analysis. Muscle fibers are present even at the core of the microtissues and on average occupy 13 ± 2.6 percent of the construct. C2C12 myotubes show well-developed striations when they are cultured on substrates with tissue-like stiffness (E approximately 12 kPa) after 2–4 weeks of differentiation (42). In a recent work, Chiron et al. cultured human myoblasts in a fibrin gel between centimeter scale elastic posts and reported the change in tissue stiffness using AFM (43). They observed that engineered skeletal muscle tissue stiffness increases upon differentiation, with E reaching 12.2 kPa. The presence of well-developed cross-striations could be explained with this change in matrix stiffness as we used a miniaturized version of the same system. Furthermore, the auxotonic load due to elastic boundary conditions (i.e. PDMS cantilevers, mimicking attachment of muscle to elastic tendons) can accelerate the muscle maturation (39).

The degree of alignment was quantified using 2D projection of images of microtissues stained for alpha-actinin. The angle was defined as the angle between the major axis of each myotube and the longitudinal axis of the construct (Fig. 3G). In the generated constructs, an orientation angle of 0° indicates perfect alignment and ± 45° represents random alignment. The average length between the caps of the microposts (l_1) was 350 μm and the average length of the microtissue (l_2) was 510 μm. When the myotube formed diagonally between the posts the orientation angle was around ± 30° (denoted by dashed blue lines in Fig. 3G), and the myotubes were as long as 550 μm if they formed on top of the caps. Figure 3H shows a scatter plot of the orientation and length of 140 myotubes from 20 different constructs. Most of the myotubes spanned almost the entire length between the microposts (79.2%). We observed occasional myotube formation that is parallel and close to the caps of the posts where the stress was not aligned with the major axis of the tissue. Data points with an orientation angle close to ± 90° represent these myotubes (Fig. 3G).

Optical stimulation of SMTs

During tissue formation, a baseline static tension is developed due to the compaction of the gel by the collective action of myoblasts. Myotubes form in the presence of this static stress, they become mature, and generate forces when stimulated. The dynamic tension is defined as the force exerted during light-activated contractions of myotubes. The amount of tension generated is calculated by measuring the cantilever deflection (Fig. 4A). At day 14 of differentiation, application of pulsed blue light reliably induced contractions of SMTs (Movie S2). The active force generated by these contractions was 1.41 ± 0.25 μN while the static tension between cantilevers was 10.8 ± 0.18 μN (Fig. 4B). These values are comparable with our previous results on spontaneously contracting cardiac microtissues generated by the same device (39). In accordance with 2D stimulation experiments, the microtissues started to contract 20.6 ± 3.2 ms after light was turned on. However, unlike 2D experiments, the duration of contraction and relaxation were consistent among SMTs, 190.9

± 11.5 ms and 279.4 ± 16.8 ms, respectively. This consistency is probably due to a more uniform maturation of myotubes within microtissues. These values are relatively long compared to the contraction durations measured in centimeter-scale skeletal muscle tissues (31, 32). This difference could be due to the stimulation protocol, properties of ECM (collagen I vs. fibrin), or the cell source (neonatal rat skeletal myoblasts vs. immortalized mouse cell line). Microtissues exposed to blue light for extended time periods become irresponsive to light stimulation for several seconds. Previous work addressed this refractory period in muscle cells and suggests that ChR2-induced sustained depolarization leads to inactivation of Na+ channels (18).

Specific tension or cross-sectional stress (i.e., tension normalized over cross-sectional area) is commonly used to compare the engineered muscle tissue with native muscle. The average cross sectional area of the SMTs was 0. 0125 mm^2 (n = 50 SMTs). The average passive cross-sectional stress was 0.864 kPa and the average active cross-sectional stress was 0.112 kPa. To obtain a better understanding of the force production potential of microtissues, we calculated the effective dynamic cross-sectional tension. The average effective cross-sectional area is the area occupied by the myotubes and this value was 0.0012 mm^2 as almost 90% of the cross-sectional area was filled by non-contractile myoblasts and collagen gel. As a result, the effective dynamic cross-sectional tension was 1.12 kPa, which is comparable to previous reports on engineered muscle tissue (31) but much lower than the native adult skeletal muscle performance (260 kPa).

Multi-DOF actuation using confined illumination

With optical stimulation, SMTs can be activated simultaneously as well as separately. One of our objectives in this study was to demonstrate multi-DOF actuation within a single engineered muscle actuator. We have already shown that myotubes grown on a surface can be activated selectively. To demonstrate multi-axes motion, we illuminated different regions of a single microtissue with blue light pulses (Movie S3). When fully stimulated, the microtissue contracted uniformly resulting in a bending of the posts as measured by the translation of the caps (Fig. 4C). All of the functional myotubes within the tissue were activated and they collectively generated 2.1 μN of dynamic tension. Alternatively, when a one side of the SMT was stimulated, only the myotubes located on that side were activated. As a result, the microtissue exhibited a torsional movement as measured by the rotation and translation of the caps (Fig. 4D, E). The dominant mode of motion in selective activation was rotation and the force generated by the contracting myotubes was measured as 0.85 μN and 0.68 μN, respectively. In the presence of diagonal myotubes (Fig. 3D), stimulation of the whole tissue resulted in both bending and torsion of the posts (Movie S2).

The optimization of actuator performance

We employed C2C12 skeletal muscle cells as they come from a well-established cell line (44), but our approach to generate optically controllable microtissues can be applied using other muscle cell types. Recent work shows that embryonic myoblasts isolated from invertebrates have the potential to perform mechanical work (45). As these cells can function at ambient conditions, they may be better suited for building robust bioactuators. Our constructs are densely packed with viable myoblasts, but only sub-population (less than 40% of the myoblasts) fuses to form functional myotubes (Fig. 3F). This non-contractile material does not produce work and adds stiffness, which impedes the optimal force output. Previous work showed that this value could be as high as 80% in engineered tissue networks (33). The superior myoblast fusion reported in (33) could be explained by the geometry of the constructs, matrix composition, or the use of primary skeletal myoblasts. Treatment of C2C12 cells with recombinant IGF-1 results in hypertrophy of differentiated myotubes on 2D surfaces (46), and the same treatment increases force generation in engineered skeletal

muscle tissues (24). In our future work, we will explore the effect of all these factors on myoblast fusion and myogenesis.

The composition of extracellular matrix (32, 47, 48) and the boundary stiffness (49) play an important role in the development and contractile force generation of an engineered muscle tissue. During development, the matrix composition affects the ability of the cells to reorganize within the tissue and the internal structure of self-assembled myotubes. The activity of the cells remodels the surrounding matrix (50). In turn, compaction of the matrix by the cells bends the elastic posts, creating a mechanical preload on each construct. This dynamic interplay among the cells, ECM and the elastic microposts determines the overall functionality of the construct. After development, the passive viscoelastic properties of the tissue determine the efficiency to store, transmit and release produced energy. In our previous study, we generated cardiac microtissues using a similar system and showed that the constructs with a denser collagen matrix (1 mg/mL vs 2.5 mg/mL) generate lower dynamic cross-sectional stress. By increasing the post stiffness, we improved the cardiac tissue development (39). Similarly, fine-tuning the matrix composition, the post stiffness and the microtissue geometry may result in an increased alignment of the myotubes and a better development of sarcomeric structure.

Skeletal muscle is one of the most adaptable (plastic) tissues in the body, and its structure and physiology change with increased or decreased use (12). Repeated electrical stimulation and cyclic stretch protocols are generally performed to exercise the engineered muscle tissues (12, 23). However, there are conflicting results in the literature and optimal stimulation parameters should be determined (51). Optical stimulation offers greater flexibility for excitation under physiological conditions. Unlike electric fields, increasing magnitude and duration of light pulses do not lead to electrochemical damage to muscle tissue (18). High-power, micro-LED arrays (52) can easily be integrated with our high-throughput device to examine the excitability and contractibility of hundreds of microtissues in real-time under various different stimulation protocols. Cyclic stretch could be applied by forming the microtissues between magnetic elastomeric cantilevers. In our previous work, we showed the feasibility of this technique by applying external forces to living cells using arrays of magnetic PDMS microposts (53).

Materials and Methods

Plasmid Contructs

pAAV-Cag-Chr2-GFP (a gift from Ed Boyden) was digested using enzymes BsrGI and EcoRI (New England Biolabs, MA). 2A-Puro was amplified with forward primer (GGACGAGCTGTACAAGGAGGGCCGCGGCAGCCTGCTGACC) and reverse primer (ATTATCGATGAATTCTCAGGCACCGGGCTTGCGGGTCATGC) that added BsrGI and EcoRI sites on the ends. The amplified PCR product was subsequently digested with BsrGI and EcoRI and ligated with the digested pAAV-Cag-Chr2-GFP to form pAAV-Cag-Chr2-GFP-2A-Puro (Fig. S1). Cloning was verified by DNA sequencing.

Cell culture and transfection

The murine-derived muscle cell line (C2C12) was purchased from American Type Culture Collection (ATCC, Manassas, VA). For the generation of transgenic cell line, C2C12-ChR2, cells were transfected with pAAV-Cag-Chr2-GFP-2A-Puro with Lipofectamine 2000 (Invitrogen, Carlsbad, CA), and were grown under Puromycin (2.5ug/ml) selection for 2 weeks. More than 98 percent of the population expresses ChR2 after selection.

For 2D stimulation experiments, C2C12-ChR2 cells were cultured in growth medium containing high-glucose DMEM (ATCC, Manassas, VA), supplemented with 10% fetal

bovine serum (FBS, Sigma, St. Louis, MO), and 1% penicillin-streptomycin (Invitrogen). When cells reach 80–90% confluency, growth medium was switched to differentiation medium containing high-glucose DMEM supplemented with 10% horse serum (Sigma, St. Louis, MO) to facilitate myotube formation and the medium is replaced every day until the termination of the experiment.

Device fabrication and microtissue seeding

We previously developed techniques to fabricate the SU-8 masters on silicon wafers (38). Multiple layers of SU-8 photoresist (Microchem) were spin-coated on a master silicon wafer to a final thickness of 250 μm. Elastomeric microtissue molds replicating the photoresist features of the patterned master wafer were created using a double-casting method. A negative replica PDMS template was first molded off the master wafer and then silanized to make it nonadhesive to further application of PDMS. The silanized template was then used to cast the final substrate that can be directly utilized as microtissue molds. The dimensions and location of the PDMS cantilevers within the wells were varied by the use of different photomasks to fabricate the corresponding masters. For force characterization experiments, we embedded fluorescent microbeads (Fluoresbrite 17147; Polysciences, Inc.) into the cantilevers to facilitate automatic tracking of cantilever deflection (39). Briefly, fluorescent bead solution (in ethanol, 3000:1) was added onto PDMS stamps inside a six-well plate and then centrifuged for 1 min at 1,000 rpm to settle the fluorescent beads into the pattern on the stamps. The ethanol was then allowed to evaporate overnight at room temperature. PDMS molds were then cast onto the stamps to produce the final uTUG substrates incorporated with fluorescent beads.

The PDMS molds were sterilized in 70% ethanol followed by UV irradiation for 15 min and treated with 0.2% (w/v) Pluronic F-127 (Invitogen) to reduce cell adhesion. A mixture of 2 mg/mL liquid neutralized collagen I from rat tail (BD Biosciences, Franklin Lakes, NJ) supplemented with 10% (v/v) Matrigel (BD Biosciences, Franklin Lakes, NJ) was then added to the surface of the substrates on ice and templates were degassed under vacuum to remove bubbles in the liquid. Matrigel was added to support faster cell spreading. A cooled suspension of cell-laden gel was then added to the substrate and the entire assembly was centrifuged to drive the cells into the micropatterned wells, resulting in approximately 400 cells per well. Excess collagen and cells were removed by dewetting the surface of the substrate before incubating at 37 °C to induce collagen polymerization. Growth medium supplemented with 50 μg/mL L-ascorbic acid (Sigma, St. Louis, MO) and 33 μg/mL aprotinin (Sigma, St. Louis, MO) were added to each device. After 4 days, growth medium was switched to the differentiation medium supplemented with 50 μg/mL L-ascorbic acid and 33 μg/mL aprotinin to induce myotube formation.

Optical stimulation in vitro

Light stimulation of single myotubes and microtissues was performed through a 20X objective with a high-power LED unit (1.5W of collimated blue light, Prizmatix) or a 300-W mercury lamp coupled with a GFP filter set (excitation wavelength 473 nm). Stimulation triggers were generated by a function generator (Agilent) or synthesized by custom software written in Metamorph and then exported to the shutter control unit. Power density of the blue light was measured with a power meter (Thorlabs).

Quantification of microtissue force and cellular displacement

Images were acquired using an inverted microscope (Olympus IX2). The contractions of myotubes (15 independent experiments) were recorded at 1 kHz using a high-speed camera (Fastcam SA2, Photron USA, Inc.) at 20X magnification. The contractile displacement was measured by tracking bright spots on the myotubes (at least 2 different points for each

myotube) using ImageJ (National Institutes of Health). For quantifying static tension, microtissues were cultured for 48 h before phase-contrast images were taken of the cantilevers within each template (45 total, 15 each from 3 independent experiments), using a CCD camera (Orca-R^2, Hamamatsu Photonics K.K., Japan). To measure dynamic forces, phase-contrast and fluorescence images were taken at 250 Hz (45 total, 15 each from 3 independent experiments), using a high-speed camera (Fastcam SA2, Photron USA, Inc.). Only tissues that were uniformly anchored to the tips of the cantilevers were included in the analysis. The displacement of the caps of the cantilevers was then tracked using ImageJ.

We calculated the spring constants of cantilevers using linear bending theory and calibrated the spring constants based on experimental measurements with a MEMS capacitive force sensor (FT-G30; Femto Tools) mounted on a micromanipulator (39). For each measurement, the sensor tip was placed 20 μm below the cap of the post, and the probe was translated laterally against the outer edge of the cantilever. Five cantilevers were measured across a substrate and measurements were repeated for three different substrates under each condition. These spring constants were then used to project the measured cantilever deflections to the amount of force generated by SMTs.

Immunofluorescence Staining and image analysis

Constructs and cells were fixed with 4% paraformaldehyde and permeabilized with 0.2% Triton X-100 (Sigma, St. Louis, MO). To visualize F-actin, cells and microtissues were directly stained with Rhodamine Phalloidin (1:100, Invitrogen) and Hoechst nuclear dye (1:1000, Invitrogen). To visualize the sarcomeric structure, microtissues were first blocked with 3% goat serum in 5% bovine serum albumin (BSA, Sigma) and incubated with primary antibodies (sarcomeric α-actinin, Sigma) overnight at 4°C. Secondary antibodies (Alexa 555, Sigma) were then applied with Hoechst nuclear dye. Images were acquired using a fluorescence microscope (Olympus IX2) or a laser scanning confocal microscope (Leica TCS SP5 II). Cell alignment was quantified from α-actinin images with ImageJ. Cross-sectional areas were estimated from z-stack images obtained with 40X water-immersion objective attached to the confocal microscope. Fine details of sarcomeric structure and actin remodeling within the myotubes were visualized using confocal images taken with 63X water-immersion objective.

Conclusion

In this work, we generated micrometer-scale, optically excitable 3D skeletal muscle bioactuators from genetically engineered mouse myoblasts expressing ChR2. We demonstrated multi-DOF motion by selectively activating individual myotubes within the microtissues using confined illumination. Our study explores the utility of optogenetics for skeletal muscle tissue engineering applications and for building a new class of muscle-powered soft robots performing biomimetic tasks. The optogenetic approach offers high spatiotemporal resolution for precise control of excitation. The presence of longitudinally aligned, cross-striated myotubes and the level of measured specific dynamic tension show that generated transgenic microtissues exhibit essential structural and functional properties of engineered skeletal muscle.

Force generation and contraction characteristics are two very important performance metrics of an engineered muscle actuator. To optimize the performance, the effects of several soluble and mechanical stimuli have to be tested experimentally in a well-controlled environment. Our system provides a non-invasive, reproducible and sensitive method to measure the forces and mechanical stresses skeletal muscle cells exert during tissue formation and twitch contractions over extended time periods using flexible cantilevers. In addition to reporting tension, these cantilevers function as artificial tendons that anchor the

microtissues. We can vary their elastic properties as well as the stiffness of the extracellular matrix simultaneously with quantitative precision. Furthermore, the dimensions of generated microtissues are small enough to allow rapid diffusion of soluble effectors and high-throughput analysis of cytoskeletal structure. Thus, using this technology, we can prepare hundreds of microtissues (130 SMTs per device) that are well-suited for examining how various different biomechanical stimuli influence the structure and function of engineered skeletal muscle bioactuators in a combinatorial manner. How to incorporate these powering units into practical robotic devices is a next technical challenge, and we are currently working on it.

Supplementary Material

Refer to Web version on PubMed Central for supplementary material.

Acknowledgments

This material was supported in part by grants from the National Science Foundation under the Science and Technology Center - Emergent Behaviors of Integrated Cellular Systems (EBICS) Grant No. CBET-0939511, the National Institutes of Health (EB00262, HL90747, GM74048), the RESBIO Technology Resource for Polymeric Biomaterials, and Center for Engineering Cells and Regeneration of the University of Pennsylvania, and Singapore-MIT Alliance of Research and Technology. We would like to thank the members of MIT Edgerton Center for their assistance in high-speed imaging.

References

1. McMahon, TA. Muscles, reflexes, and locomotion. Princeton Univ Press; Princeton, NJ: 1984.
2. Van Ham R, Sugar TG, Vanderborght B, Hollander KW, Lefeber D. Compliant actuator designs. IEEE Robotics and Automation Magazine. 2009; 16:81–94.
3. Dennis, RG.; Herr, H. Biomimetrics: biologically inspired technologies. CRC Press; New York, NY: 2005. p. 243-266.
4. Nawroth JC, Lee H, Feinberg AW, Ripplinger CM, McCain ML, Grosberg A, et al. A tissue-engineered jellyfish with biomimetric propulsion. Nat Biotech. 201210.1038/nbt.2269
5. Feinberg AW, Feigel A, Shevkoplyas SS, Sheehy S, Whitesides GM, Parker KK. Muscular Thin Films for Building Actuators and Powering Devices. Science. 2007; 317:1366–1370. [PubMed: 17823347]
6. Xi J, Schmidt JJ, Montemagno CD. Self-assembled microdevices driven by muscle. Nat Mater. 2005; 4:180–184. [PubMed: 15654345]
7. Kim J, Park J, Yang S, Baek J, Kim B, Lee SH, et al. Establishment of a fabrication method for a long-term actuated hybrid cell robot. Lab Chip. 2007; 7:1504–1508. [PubMed: 17960278]
8. Tanaka Y, Sato K, Shimizu T, Yamato M, Okano T, Kitamori T. A micro-spherical heart pump powered by cultured cardiomyocytes. Lab Chip. 2007; 7:207–212. [PubMed: 17268623]
9. Pilarek M, Neubauer P, Marx U. Biological cardio-micro-pumps for microbioreactors and analytical micro-systems. Sens Actuators B. 2011; 156:517–526.
10. Chan V, Jeong JH, Bajaj P, Collens M, Saif T, Kong H, et al. Multi-material bio-fabrication of hydrogel cantilevers and actuators with stereolithography. Lab Chip. 2012; 12:88–98. [PubMed: 22124724]
11. King AM, Loiselle DS, Kohl P. Force generation for locomotion of vertebrates: Skeletal muscle overview. IEEE J Oceanic Eng. 2004; 29:684–691.
12. Lieber, RL. Skeletal muscle structure, function, and plasticity: the physiological basis of rehabilitation. Lippincott Williams & Wilkins; 2010.
13. Keynes, RD.; Aidley, DJ.; Huang, CL-H. Nerve and muscle. Cambridge Uni Press; NY: 2011.
14. Dickinson MH, Farley CT, Full RJ, Koehl MAR, Kram R, Lehman S. How animals move: an integrative view. Science. 2010; 288:100–106. [PubMed: 10753108]

15. Nagamine K, Kawashima t, Sekine S, Ido Y, Kanzaki M, Nishizawa M. Spatiotemporally controlled contraction of micropatterned skeletal muscle cells on a hydrogel sheet. Lab Chip. 2011; 11:513–517. [PubMed: 21116545]
16. Zhang F, Wang L-P, Boyden ES, Deisseroth K. Channelrhodopsin-2 and optical control of excitable cells. Nat Methods. 2006; 3:785–792. [PubMed: 16990810]
17. Fenno L, Yizhar O, Deisseroth K. The development and application of optogenetics. Annu Rev Neurosci. 2011; 34:389–412. [PubMed: 21692661]
18. Bruegmann T, Malan D, Hesse M, Beiert T, Fuegemann CJ, Fleischmann BK, et al. Optogenetic control of heart muscle in vitro and in vivo. Nat Methods. 2010; 7:897–900. [PubMed: 20881965]
19. Arrenberg AB, Stainier DY, Baier H, Huisken J. Optogenetic control of cardiac function. Science. 2010; 330:971–974. [PubMed: 21071670]
20. Nagel G, Brauner M, Liewald JF, Adeishvili N, Bamberg E, Gottschalk A. Light activation of channelrhodopsins-2 in excitable cells of Caenorhabditis elegans triggers rapid behavioral responses. Current Biology. 2005; 15:2279–2284. [PubMed: 16360690]
21. Stirman JN, Crane MM, Husson SJ, Wabnig S, Schultheis C, Gottschalk A, et al. Real-time mutimodal optical control of neurons and muscles in freely behaving Caenorhabditis elegans. Nat Methods. 2011; 8:152–58.
22. Leifer AM, Fang-Yen C, Gershow M, Alkema MJ, Samuel ADT. Optogenetic manipulation of neural activity in freely moving Caenorhabditis elegans. Nat Methods. 2011; 8:147–152. [PubMed: 21240279]
23. Dennis RG, Smith B, Philip A, Donnely K, Baar K. Bioreactors for guiding muscle tissue growth and development. Adv Biochem Eng Biotechnol. 2009; 112:39–79. [PubMed: 19290497]
24. Vandenburgh H, Shansky J, Benesch-Lee F, Barbata V, Reid J, Thorrez L, et al. Drug-screening platform based on the contractility of tissue-engineered muscle. Muscle Nerve. 2008; 37:438–447. [PubMed: 18236465]
25. Vandenburgh H. High-content drug screening with engineered musculoskeletal tissues. Tissue Eng: Part B. 2010; 16:55–64.
26. Vandenburgh H, Swasdison S, Karlisch P. Computer-aided mechanogenesis of skeletal muscle from single cells in vitro. FASEB J. 1991; 5:2860–2867. [PubMed: 1916108]
27. Okano T, Satoh S, Oka T, Matsuda T. Tissue engineering of skeletal muscle. Highly dense, highly oriented hybrid muscular tissues biomimicking native tissues. Asaio J. 1997; 43:M749–53. [PubMed: 9360146]
28. Dennis RG, Kosnik PE. Excitability and isometric contractile properties of mammalian skeletal muscle constructs engineered in vitro. In Vitro Cell Dev Biol Anim. 2000; 36:327–335. [PubMed: 10937836]
29. Huang YC, Dennis RG, Larkin L, Baar K. Rapid formation of functional muscle in vitro using fibrin gels. J Appl Physiol. 2005; 98:706–713. [PubMed: 15475606]
30. Rhim C, Lowell DA, Reedy MC, Slentz DH, Zhang SJ, Kraus WE, et al. Morphology and ultrastructure of differentiating three-dimensional mammalian skeletal muscle in a collagen gel. Muscle Nerve. 36:71–80. [PubMed: 17455272]
31. Lam MT, Huang Y-C, Birla RK, Takayama S. Microfeature guided skeletal muscle tissue engineering for highly organized 3-dimensional free-standing constructs. Biomaterials. 2009; 30:1150–1155. [PubMed: 19064284]
32. Hinds S, Bian W, Dennis RG, Bursac N. The role of extracellular matrix composition in structure and function of bioengineered skeletal muscle. Biomaterials. 2011; 32:3575–3583. [PubMed: 21324402]
33. Bian W, Bursac N. Engineered skeletal muscle tissue networks with controllable architecture. Biomaterials. 2009; 30:1401–1412. [PubMed: 19070360]
34. Bian W, Liau B, Badie N, Bursac N. Mesoscopic hydrogel molding to control the 3D geometry of bioartificial muscle tissue. Nat Protocols. 2009; 4:1522–1534.
35. Bian W, Juhas M, Pfeiler TW, Bursac NN. Local tissue geometry determines contractile force generation of engineered muscle networks. Tissue Eng: Part A. 2012; 18:957–967. [PubMed: 22115339]

36. Alford PW, Feinberg AW, Sheehy SP, Parker KK. Biohybrid thin films for measuring contractility in engineered cardiovascular muscle. Biomaterials. 2010; 31:3613–3621. [PubMed: 20149449]
37. Grosberg A, Alford PW, McCain ML, Parker KK. Ensembles of engineered cardiac tissues for physiological and pharmacological study: Heart on a chip. Lab Chip. 2011; 11:4165–4173. [PubMed: 22072288]
38. Legant WR, Pathak A, Yang MT, Deshpande VS, McMeeking RM, Chen CS. Microfabricated tissue gauges to measure and manipulate forces from 3D microtissues. Proc Natl Acad Sci USA. 2009; 106:10097–10102. [PubMed: 19541627]
39. Boudou T, Legant WR, Mu A, Borochin MA, Thavandian N, Radisic M, et al. A microfabricated platform to measure and manipulate the mechanics of engineered cardiac microtissues. Tissue Eng: Part A. 201210.1089/ten.tea.2011.0341
40. Asano T, Ishizua T, Yawo H. Optically controlled contraction of photosensitive skeletal muscle cells. Biotech Bioeng. 2012; 109:199–204.
41. Jia Z, Valiunas V, Lu Z, Bien H, Liu H, Wang H-Z, et al. Stimulating cardiac muscle by light: cardiac optogenetics by cell delivery. Circ Arrhythm Electrophysiol. 2011; 4:753–760. [PubMed: 21828312]
42. Engler AJ, Griffin MA, Sen S, Bonnemann CG, Sweeney HL, Discher DE. Myotubes differentiate optimally on substrates with tissue-like stiffness: pathological implications for soft or stiff microenvironments. J Cell Biol. 2004; 166:877–887. [PubMed: 15364962]
43. Chiron S, Tomczak C, Duperray A, Laine J, Bonne G, Eder A, et al. Dynamic interplay between human myoblasts and 3D fibrin-based matrix. PLoS ONE. 2012; 7:e36173. [PubMed: 22558372]
44. Yaffe D, Saxel O. Serial passaging and differentiation of myogenic cells isolated from dystrophic mouse cells. Nature. 1977; 270:725–727. [PubMed: 563524]
45. Baryshyan AL, Woods W, Trimmer BA, Kaplan DL. Isolation and maintanance-free culture of contractile myotubes from mandura sexta embryos. PLoS ONE. 2012; 7:e31598. [PubMed: 22355379]
46. Semsarian C, Wu M-J, Ju Y-K, Marciniec T, Teoh T, Allen DG, et al. Skeletal muscle hypertrophy is mediated by a Ca^{2+}-dependent calcineurin signaling pathway. Nature. 1999; 400:576–581. [PubMed: 10448861]
47. Levy-Mishali M, Zoldan J, Levenberg S. Effect of scaffold stiffness on myoblast differentiation. Tissue Eng: Part A. 2009; 15:935–944. [PubMed: 18821844]
48. Boontheekul T, Hill EE, Kong H-J, Mooney DJ. Regulating myoblast phenotype through controlled gel stiffness and degradation. Tissue Eng. 2007; 13:1431–1442. [PubMed: 17561804]
49. Zimmermann W-H, Melnychenko I, Wasmeier G, Didie M, Naito H, Nixdorff U, et al. Engineered heart tissue grafts improve systolic and diastolic function in infracted rat hearts. Nat Med. 2006; 12:452–458. [PubMed: 16582915]
50. Dado DD, Levenberg S. Cell-scaffold mechanical interplay within engineered tissue. Seminars in Cell & Developmental Biology. 2009; 20:656–664. [PubMed: 19596326]
51. Khodabukus A, Baar K. Defined electrical stimulation emphasizing excitability for the development and testing of engineered skeletal muscle. Tissue Eng: Part C. 2012; 18:349–357.
52. Grossman N, Poher V, Grubb MS, Kennedy GT, Nikolic K, McGovern B, et al. Multi-site optical excitation using ChR2 and micro-LED array. J Neural Eng. 2010; 7:016004.
53. Sniadecki NJ, Anguelouch A, Yang MT, Lamb CM, Liu Z, Kirschner SB, et al. Magnetic microposts as an approach to apply forces to living cells. Proc Natl Acad Sci USA. 2007; 104:14553–14558. [PubMed: 17804810]

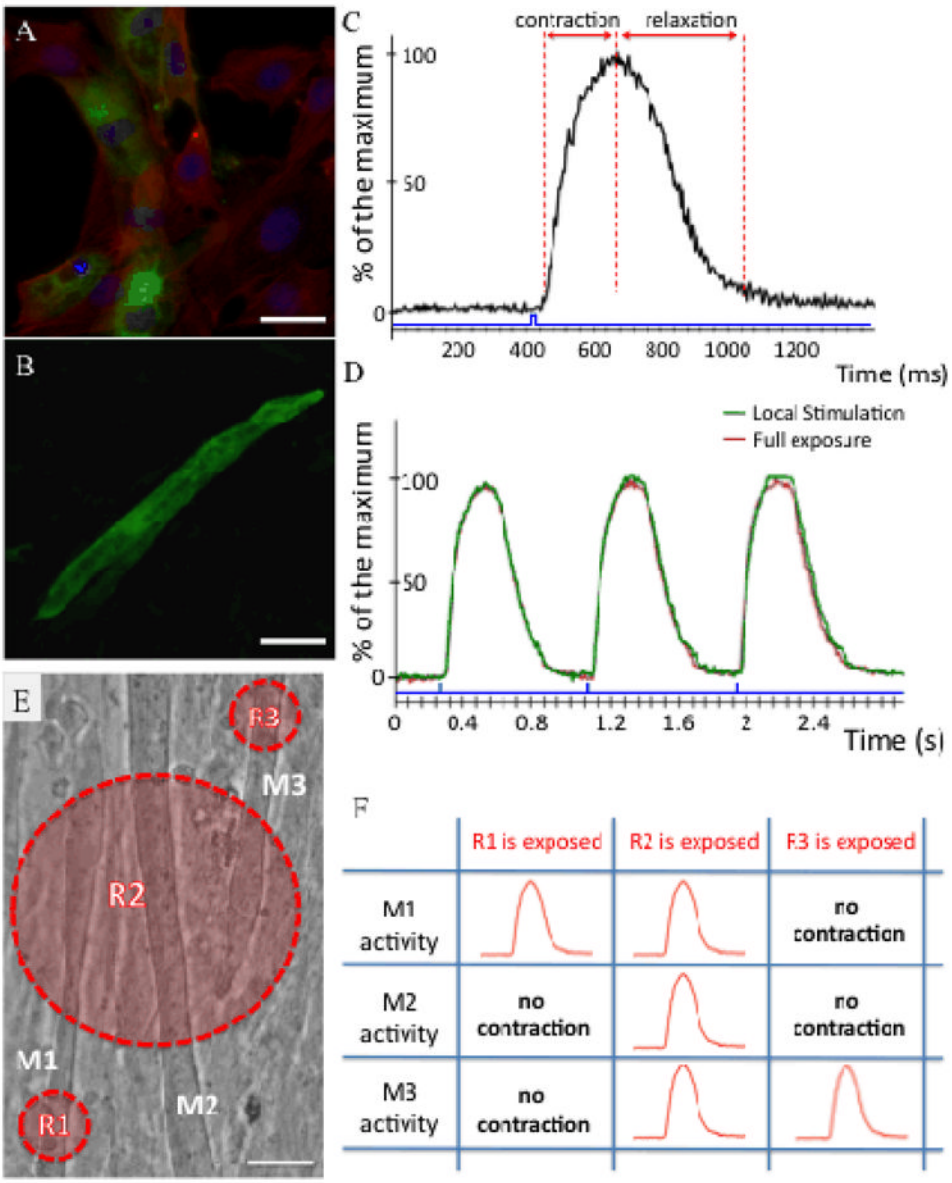

Figure 1.

Generation and light-induced stimulation of ChR2-expressing skeletal muscle cells *in vitro*. (A) Fluorescence image of the membrane-bound ChR2-GFP signal (green) overlaid with F-actin immunostaining (red) in C2C12 myoblasts. Nuclei are shown in blue. (B) Multi-nucleated myotubes expressing the GFP signal (green). (C) Typical contraction pattern of a ChR2-GFP expressing myotube upon stimulation with blue light pulses (10 mW mm^{-2}) for durations indicated by blue bars. A representative example of 20 experiments is shown. (D) Representative repetitive contraction pattern evoked by local and full exposure of a ChR2-GFP–expressing myotube with blue light pulses (10 mW mm^{-2}) for durations indicated by blue bars. (E) Selective activation of myotubes with local stimulation. Myotubes are denoted by M1, M2 and M3 and regions of exposure are labeled with R1, R2, and R3. (F) Blue light pulses confined to a region stimulate only the myotubes residing inside that specific region. (Scale bars: A, 10 μm; B and E, 20 μm).

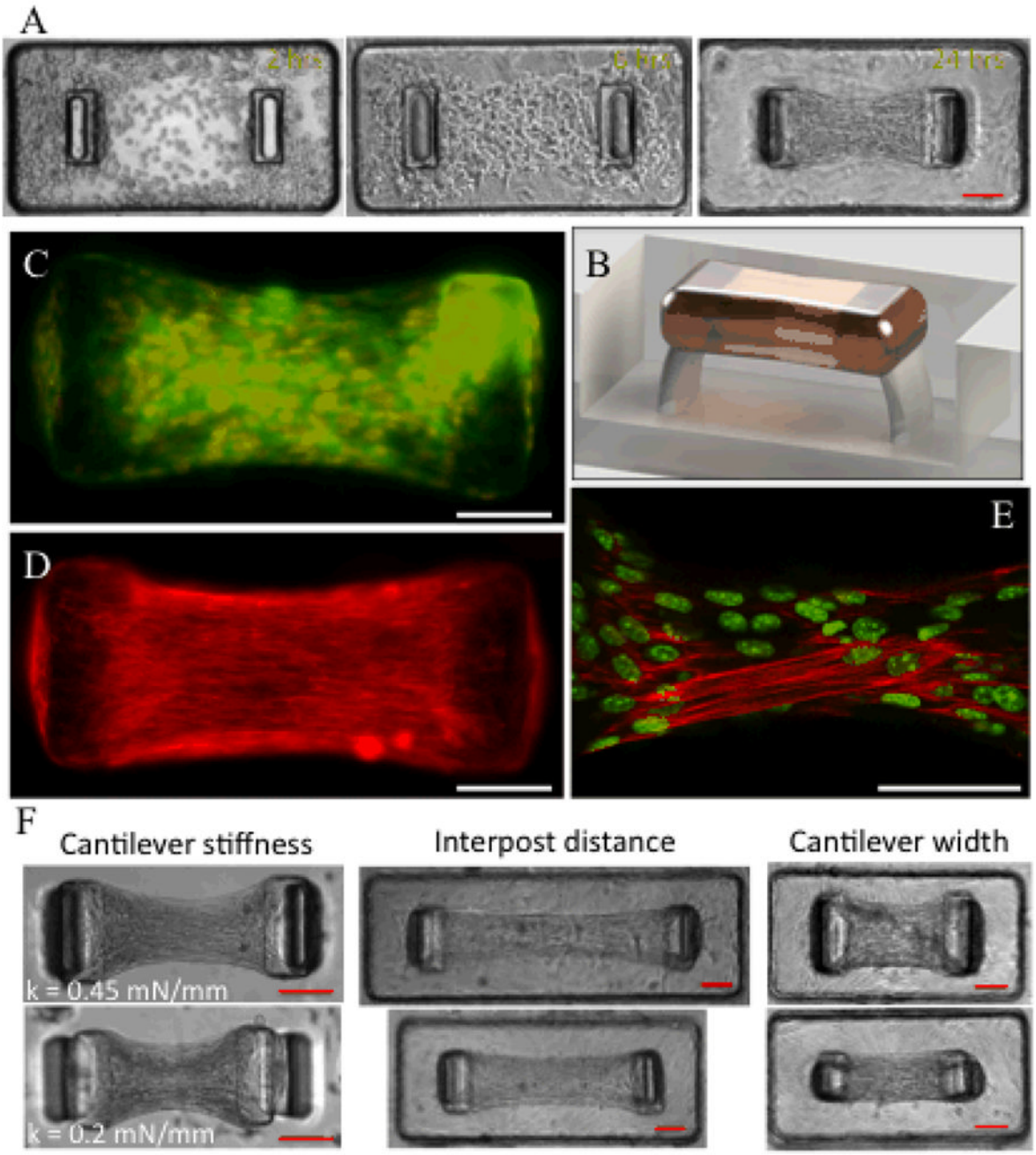

Figure 2.

Generation of skeletal muscle microtissues (SMTs) tethered to elastic force sensors. (A) Representative images depicting the time course of a contracting SMT. (B) Cross section view of the CAD modeling of a single SMT. (C) Representative immunofluorescence overlay of membrane-bound GFP signal (green) and nuclei staining (red) within microtissues showing uniform cell distribution. (D) Representative F-actin imaging (red) revealing the alignment of skeletal muscle myoblasts in the direction of mechanical stress gradients within the microtissues after 3 days of culture. (E) Remodeling of actin (red) within multi-nucleated myotubes. Nuclei are shown in green. (F) Effect of PDMS cantilever

stiffness and device geometry on the skeletal muscle microtissue dimensions. (Scale bars: 100 μm).

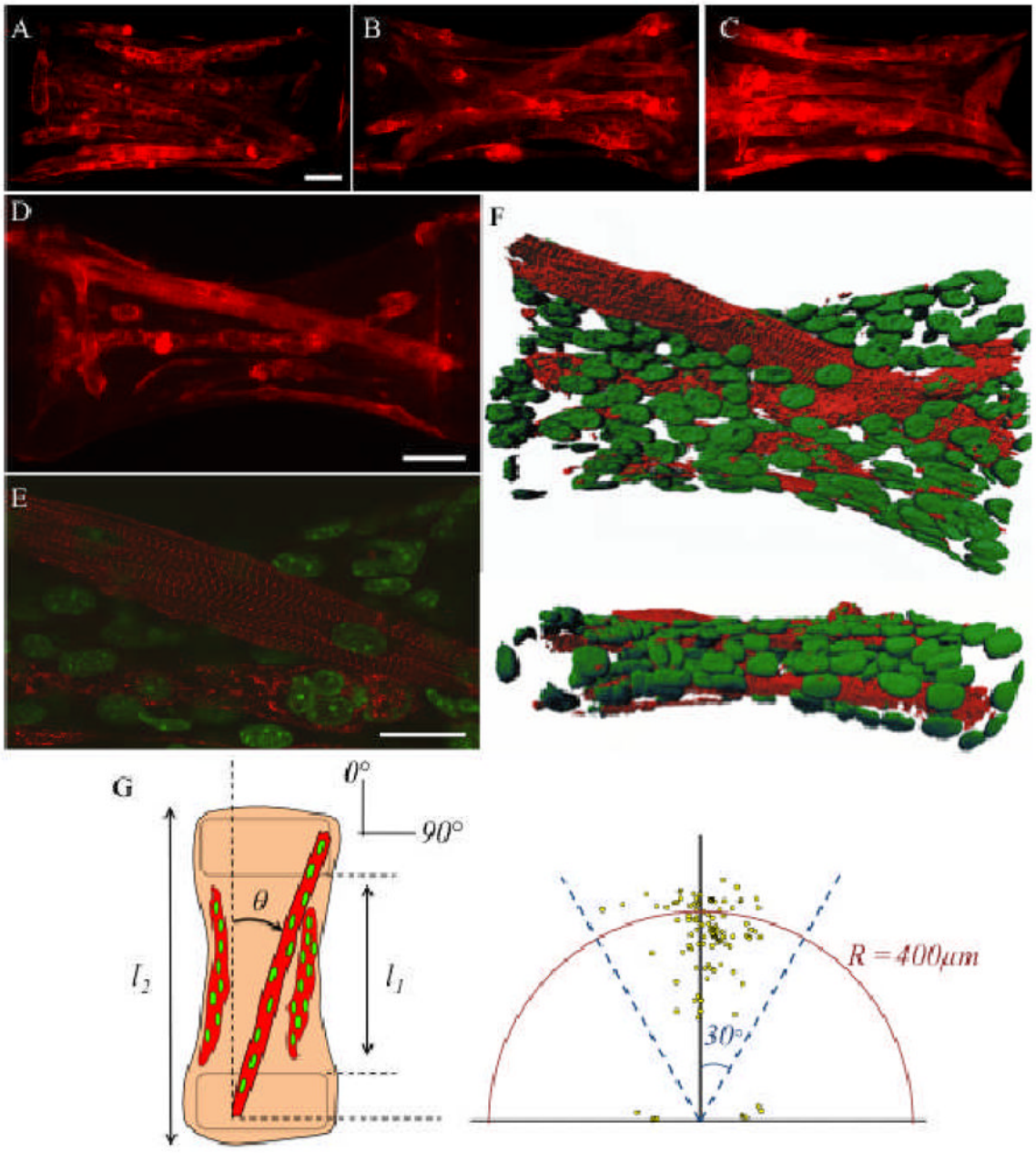

Figure 3.

Distribution and differentiation of skeletal muscle myotubes in engineered microtissues. (A–C) Representative α-actinin immunostaining images showing the distribution and alignment of striated myotubes after 3 weeks of culture. (D) Representative α-actinin immunostaining image shows sarcomere formation and (E) a representative confocal section from the same construct shows that aligned multinucleated myotubes exhibit ubiquitous cross-striations. (F) 3D reconstruction of confocal slices for the construct shown in (D). The upper panel shows the top and the lower panel shows the side view of the same microtissue. Nuclei (green) are elongated in the direction of stress gradients. (G) Characterization of cell alignment and myotube length in the microtissues. The location of each point in the scatter plot shows the length and orientation of a myotube. Data are collected from 20 SMTs having a total of 150 myotubes. (Scale bars: A and D, 50 μm; E, 25 μm).

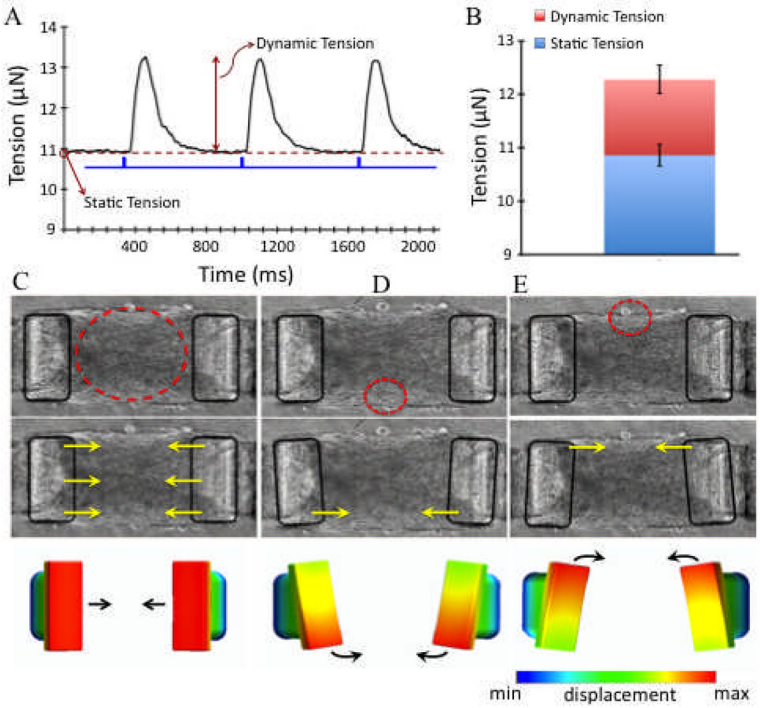

Figure 4.

Functional properties of SMTs and multi degrees of freedom actuation with local stimulation (A) Representative recording of the static and dynamic tension of an SMT on day 15. The microtissue is stimulated with a brief blue light pulse series (indicated by blue bars). (B) Average static and dynamic tension for SMTs at day 15. Data are the average of 50 SMTs ± SEM. (C–E) Multi DOF actuation. Caps are outlined with black rectangles to emphasize motion. Heat maps depicting degree of displacement.